A New Convex Approach for Grid-Supporting Inverter Control Based On DLMIs

Roberto M. Fuentes *Students, IEEE*, Esteban I. Marciel *Students, IEEE*, Carlos R. Baier *Senior, IEEE*, Gabriela W. Gabriel, Cecilia F. Morais, Márcio J. Lacerda *Senior, IEEE*, and Jonathan M. Palma *Member, IEEE*.

***Abstract*— The objective of this paper is to validate a dynamic output-feedback (DOF) control synthesis methodology to be implemented through digital signal processors (DSPs) in the scope of electrical microgrid applications. The DOF controller, originally designed in continuous-time, is developed aiming to comply with strict transient behavior requirements associated with electrical systems, by using an adaptation of the $\mathcal{D}$-stability concept to handle linear systems affected by time-varying parameters (linear parameter varying - LPV - model). In order to allow a digital implementation of the control action, a discrete-time equivalent representation of the continuous-time DOF controller is obtained from the Taylor series expansion of the exponential terms associated with the discretization. Additional contributions of this article include: the use of a formulation based on Differential Linear Matrix Inequalities (DLMIs) to ensure the stability of the hybrid system (composed of the analog plant and the digital controller), and the validation of the redesigned controller performance when applied to a real-time simulation of a three-phase inverter with a grid-supporting configuration emulated via Hardware-in-the-loop (HIL) device. The results demonstrate that the controlled system has achieved a regular operation for all the load cases investigated after the anomalies presented, even regulating a voltage drop of 20%. The proposed method was compared with a method in the literature, showing a decrease of 17.5% in the harmonic distortion of the currents holding similar voltage distortion.**

***Index Terms*— Digital Redesign, DLMI, Dynamic output-feedback, Grid-supporting, Hybrid Systems Stability, Inverter.**

I. Introduction

IN electrical distribution grids, there has been a shift from the use of environmentally unfriendly energy generation sources to unconventional renewable energy sources such as solar and wind [1]. The transmission of the energy produced by photovoltaic-based generators through the current electrical distribution requires its conversion from direct current to alternating current, which can be achieved through power electronic-based energy converters [2].

The grid-tied converters can use three types of operation: grid-following converter, which functions as a current source aiming to deliver the maximum amount of energy to an electrical grid [3], grid-forming inverter, which operates as a voltage source, allowing voltage and frequency control to maintain grid or microgrid stability [4], and grid-supporting inverter, which provides support services to the electrical grid by operating as a current or voltage source, depending on the services desired for the grid [5]. The grid-tied power converters need to be controlled to avoid failures and to maintain the stability of the power and voltage signals, along with a good performance associated with low tracking error and low harmonic distortion. This ensures that converters have only a positive effect on the grid. In this sense, several approaches have been developed to achieve better performance or provide additional functionalities to the converter system [6].

In the literature, various strategies are used to control the output of converters, such as the output current, the voltage in a filter, or the current delivered to the grid (according to the study case). These strategies can be implemented considering a single loop or a double loop, depending on the number of variables measured and controlled [7]. Single-loop control methods use multiple modulation-based strategies to generate semiconductor activation signals. In past decades, proportional (P) control has been used despite being prone to steady-state error problems [8]. On the other hand, proportional-integral (PI) control eliminates steady-state error when working in the dq reference frame for AC systems [9]; proportional-resonant (PR) control [10], [11], one of the most used due to its ability to eliminate steady-state error when working with alternate variables, allows to work in abc [12] and $\alpha\beta$ [13] frames; additionaly, deadbeat control (DB) [14] uses estimation to achieve the minimum possible error [15].

Also, there are modulation-free strategies such as Model Predictive Control (MPC) strategies, where the controller's output is the direct activation signal of the semiconductors. These strategies take advantage of the discrete nature of converters to estimate variables based on different semiconductor activation combinations [16]. When used alone in the feedback control loop, all the aforementioned strategies

(Corresponding author: Jonathan M. Palma).

R.M.F and E.I.M are with the Engineering Systems Doctoral Program, Faculty of Engineering, Universidad de Talca, 3340000 Curicó, Chile (e-mail:roberto.fuentes@utalca.cl, esteban.marciel@utalca.cl).

C.R.B. and J.M.P. are with the Department of Electrical Engineering, Faculty of Engineering, Universidad de Talca, Curicó, 334000, Chile (e-mail: cbaier@utalca.cl, jonathan.palma@utalca.cl).

G.W.G is with the Divisão de Engenharia Eletrônica, Instituto Tecnológico de Aeronáutica, São José dos Campos 12228-900, Brazil (e-mail: ggabriel@ita.br).

C.F.M. is with the Fac. de Eng. Elétrica e de Computacão Univ. Estadual de Campinas (UNICAMP) 13083-852 Campinas, SP, Brazil (e-mail:cfmorais@unicamp.br).

M.J.L is with the School of Computing and Digital Media, London Metropolitan University, London, N7 8DB, UK (email:m.lacerda@londonmet.ac.uk).

present problems such as variable switching frequency, higher harmonic distortion, or even generating resonances in weak grids [17]. Therefore, variations of these strategies, where fixed switching frequencies are used, are also under investigation [18]. In the case of double-loop strategies in power converters, an outer loop is usually implemented to generate the reference for the single-loop strategy, creating a cascaded structure that allows greater flexibility in control. These loops typically measure two of the converter's outputs dedicated to control, where the outer loop usually receives a static reference or an output from a power control. Double loops can be used similarly to single loops, combining P, PI, PR, and DB type strategies [7]. In this sense, feedback controller families often offer an integral solution because they incorporate more than one variable simultaneously in the control signal calculation.

In the feedback control framework, there are three main structures suitable for state space representations (listed below, in ascending order, according to implementation complexity) [19]–[21]: the State-Feedback (SF) controller, the Static Output-Feedback (SOF) controller, and the Dynamic Output-Feedback (DOF) controller. The static structures (SF and SOF) do not increase the order of the closed-loop system, whereas the DOF does while static structures (SF and SOF) do not modify the order of the closed-loop system, as they are fixed matrix gains, the DOF controller is a system with its own dynamics that uses the measured output to compute the temporal evolution of an arbitrary number of internal states (increasing the order of the closed-loop system) and, from them, determine the control signal. In terms of control structures, DOF is the most general one; therefore, any other structure based on compute-by-gains (PID family included) is a particular case of a DOF controller. The benefits of using a DOF control strategy in power electronic systems when compared with static approaches, such as SF, MPC, DB, or even PID family for higher than second-order systems, are that the DOF controller can provide an active disturbance rejection because it can consider the disturbance model inside the system structure and it can work with noisy measurement signals [22] since the inner dynamic of the controller can filter the high-frequency noise from lower-precision instruments. Moreover, the DOF controller is computed offline, demanding less computational effort when compared to the MPC technique. Unfortunately, as much as the DOF controller is complete, it is also complex to synthesize. In robust control, a common strategy to obtain DOF controllers is to use Lyapunov stability concept and rewrite the design problems in the form of Linear Matrix Inequalities (LMIs) in order to allow the employment of the available optimization tools, aiming to facilitate the search for a feasible solution that simultaneously guarantees the asymptotic stability of the closed-loop system and ensures the optimization of a performance criterion. We usually find LMI-based control synthesis in the literature in the following way: continuous-time controllers designed for continuous-time models or discrete-time controllers designed for discrete-time models. However, it is important to note that in real electronic applications, the system is a continuous-time process while the controller must be implemented in a discrete-time device. Hence, in some instances, an approximation of the system or the controller must be made. This process may not ensure a correct mapping of the continuous-time domain properties into their discrete-time equivalent domain. This problem is addressed in the context of hybrid systems, for example [23], [24], where the DOF control and the filtering problems in the context of sampled-data systems are solved using Differential Linear Matrix Inequalities (DLMI), respectively, without considering performance requirements. For a closed-loop stability check, the impulsive approach presented in [25] can be used, which also leads to a DLMI formulation. To solve DLMI problems using standard LMI solvers, additional mathematical features are needed, as discussed in [26]. Unfortunately, the closer topic that addresses transient state in LMI-based control theory is employing the $\mathcal{D}-$stability framework, but when hybrid systems are considered, there is no direct equivalency between the classical approach and the sampled-data approach, since the $\mathcal{D}-$stability framework relies on the concept of poles and zeros, and the restriction in its placement. In sampled-data Hybrid Linear System (HLS), this concept is not immediate, therefore, it is important to propose alternative ways to achieve transient performance when a digital controller is used, because ensuring accurate mapping of properties in the discrete-time domain is crucial for systems that require both transient- and steady-state performance.

A recent paper [27], hereinafter called FLMOP24, addresses the transient- and steady-state performance in continuous-time power electronic systems, proposing a DOF control design as the main contribution, it handles the discretization problem, including a model of the digitizing error as a perturbation to reduce its effect when the controller is implemented in a digital device. Although this methodology offers satisfactory results, it requires statistical information that is not commonly available *a priori*. An alternative is to employ a stability test based on hybrid-time modeling to avoid the requirement of statistical information and ensure the performance of a sampled-data controller that is implemented on a digital device. Hence,

Notation: Lowercase and capital letters indicate, respectively, vectors (or scalars) and matrices. The set of real numbers is denoted by $\mathbb{R}$, while the natural numbers are given by $\mathbb{N}$. For real matrices and vectors, the symbol $(')$ represents transposition, $\mathrm{He}(M)$ is used to indicate operation $M + M'$, Newton's notation is used to denote derivatives, where $\dot{f}(t)$ represents the derivative with respect to the time of the function $f(t)$. The expressions $M_1 \succ 0$ and $M_2 \prec 0$ indicate that M_1 is positive definite and M_2 is negative definite. The parameter-dependent matrices are structured in the form $X(\theta(t)) = X_0 + \sum_{i=1}^{V} X_i\theta_i(t)$, where X_i, $i = 0, \ldots, V$, are known matrices, and $\theta(t)$ is a vector of bounded time-varying parameters belonging to the set $\Theta(t) = \left\{(\theta_1, \ldots, \theta_V)(t) \in \mathbb{R}^V : \underline{\theta_i} \leqslant \theta_i \leqslant \overline{\theta_i},\ i = 1, \ldots, V\right\}$, for all $t \geqslant 0$. Moreover, the bounds $\underline{\theta_i}$ and $\overline{\theta_i}$ are known values. A trajectory or function f evaluated at $t = t_k$ is denoted as $f[k] = f(t_k), \forall k \in \mathbb{N}$.

Concerning stand electrical nomenclature, R_f, L_f and C_f are the filter resistance, inductance, and capacitance; E_{abc} is the inverter output voltage; $I_{0,dq}$ is the inverter output current; i_{abc} and v_{abc} represent the filter current and voltage in $abc-$frame, respectively, while i_{dq} and v_{dq} indicates these magnitudes in $dq-$frame; m_{dq} is the modulation signal; $\omega*$ and ω_0 represent the nominal and instantaneous value of the grid frequency; and F_{sw} is the switching frequency. About general abbreviations, DG is Distributed Generation; DLMI is Differential Linear Matrix Inequalities; DOF is Dynamic Output-Feedback; DSP is Digital Signal Processor; HIL is Hardware-in-the-Loop; HLS is Hybrid Linear System; LMI is Linear Matrix Inequality; LPV is Linear Parameter-Varying; MPC is Model Predictive Control; P, PI, PR, PID refers to Proportional-Integral-Differential-Resonant controllers family; PCC is Point of Common Coupling; PLL is Phase-Locked Loop; SF is State-Feedback; SOF is Static Output-Feedback; and THD is Total Harmonic Distortion.

the main contributions of this article are as follows.

1) We propose an offline algorithm for designing DOF controllers for discrete-time LPV systems based on the discrete-time redesign holding the improvement transient behavior outlined for a continuous-time $\mathcal{D}$-stable DOF controller.
2) In the proposed algorithm, we are able to ensure the stability of the hybrid system (continuous-time plant plus discrete-time DOF controller), through the solution of a feasibility problem based on DLMIs.
3) Finally, we validate the proposed methodology through the implementation of DOF-designed controllers with transient behavior on a DSPs and HIL apparatus.

The paper is organized as follows. Section II describes the system in an adequate mathematical framework and proposes a discrete-time approach to be implemented in real applications, considering $\mathcal{D}$-stability requirements and hybrid format. Section III presents the state-space model of the microgrid inverter system. Section IV describes the controlled system model with the presentation of a complete schema. Section V explains the experimental setup and shows the results of the proposed control methodology. Finally, Section VI resumes the main conclusions of the work.

II. Description of System Dynamics

A power electronic converter based on semiconductor switching technology can be modeled by a nonlinear system with specific behavior requirements, in which the voltage and current are the state variables. Regarding the concept of stability and performance in nonlinear systems, when a continuous-time system is redesigned into a discrete-time system, this tends to lose information about the original domain. Therefore, synthesizing the controller in a continuous-time domain offers a more representative closed-loop behavior. In this case, later a discretization is necessary. This approach may not guarantee the requirements, even the stability of the real system, which is hybrid by construction. A continuous-time system (represented by the set $\mathcal{G}$) is composed of a finite state vector $x(t)$, a control signal vector $u(t)$, an exogenous disturbance input vector $w_c(t)$, which is useful for measuring the impact of the system on the output vector $z(t)$. This output can be represented as a linear combination of the state vector, control vector, and disturbance input vectors, and it is used to generate a quadratic cost. Considering that the power converter system $\mathcal{G}$ is modeled using averaging value methods (approximated by a small-signal average), it is crucial to recognize that this approach precludes a more exact representation. This limitation stems from the inherent high-frequency switching deviations in semiconductors, which are integral to the real system. Such deviations are characterized and defined by the measurement $y[k]$. After the detailed description presented before, consider that the power converter system $\mathcal{G}$ is represented by the following Linear Parameter-Varying (LPV) sampled-data system in the standard form

$$\mathcal{G}:\begin{cases}\dot{x}(t) = & A(\theta(t))x(t)+B(\theta(t))u(t)+J(\theta(t))w_c(t),\\ z(t) = & C_z(\theta(t))x(t)+D_z(\theta(t))u(t)+E_z(\theta(t))w_c(t),\\ y(t) = & y[k],\forall t\in[t_k,t_{k+1})\end{cases} \tag{1}$$

where $x(t)\in\mathbb{R}^n$ is the state vector, $w_c(t)\in\mathbb{R}^{p_c}$ is the exogenous continuous-time disturbance, $z(t)\in\mathbb{R}^q$ is the regulated output and $y(t)\in\mathbb{R}^m$ is the piecewise constant output signal measured at the sampling times and held constant until the next sampling. Additionally, $u(t)\in\mathbb{R}^e$ is the control input, which is also a piecewise constant signal defined by $u(t)=u[k], t\in[t_k,t_{k+1}],\forall k\in\mathbb{N}$, with $t_{k+1}-t_k=h>0,\forall k\in\mathbb{N}$, being h constant. It is important to stress that although the system $\mathcal{G}$ is presented in the continuous-time domain, the control signal is piecewise constant since the control signal is implemented by a Digital Signal Processor (DSP). It is important to mention that it is possible to consider a continuous-time control device, but it leads to high maintenance and installation costs. Since the controller device is digital, the measured output is read by the controller following the sequence of sampling instants $\{t_k\}_{k\in\mathbb{N}}$, generating the measured output sampled

$$y(t_k)=C_y(\theta(t_{k-1}))x(t_{k-1})+E_y(\theta(t_{k-1}))w_d[k-1] \tag{2}$$

where $w_d\in\mathbb{R}^{p_d}$ is a discrete-time exogenous input introduced by the sensors. For this scenario, there are common proposals of control schemes based on states observer (SO), SOF, and DOF, whose goal is optimizing the output $z(t)$ (which can be any chosen linear combination of states) to minimize the effect of a noisy measurement signal, but without considering additional $\mathcal{D}$-stability requirements in the design problem.

In this paper, a noisy reject strategy is used, and therefore, we aim to design a full-order discrete-time DOF control structure given by

$$\mathcal{C}_k:\begin{cases}x_{\mathcal{C}_k}(t_k) = & A_{\mathcal{C}_k}(\theta(t_{k-1}))x_{\mathcal{C}_k}(t_{k-1})+B_{\mathcal{C}_k}(\theta(t_{k-1}))y(t_k),\\ u(t_{k-1}) = & C_{\mathcal{C}_k}(\theta(t_{k-1}))x_{\mathcal{C}_k}(t_{k-1})+D_{\mathcal{C}_k}(\theta(t_{k-1}))y(t_k),\end{cases} \tag{3}$$

where $x_{\mathcal{C}_k}(t)\in\mathbb{R}^n$ is the state vector of the dynamic controller.

As mentioned in the Introduction, the controller $\mathcal{C}_k$ described by (3) (implemented through the microprocessor in Fig. 1) uses the system output signal to feed the internal states of the controller. The output of the controller matches the control input signal of the system, which is generated by a linear combination of the internal controller states and the system output vector. When a power electronic system employs a double-loop PI controller for tracking-reference purposes, the integral and proportional actions operate over the reference-error signal twice. In contrast, the DOF controller holds an integral action over the reference-error signal and the states vector directly, plus the proportional actions, which leads to more feedback-information to generate the control signal. It can be easily seen that the proposed feedback control system (see Fig. 1) corresponds to a hybrid system composed of discrete-time and continuous-time signals. The representation of this system in state-space considering (1), (2), and (3) is given by Fig. 1. For that, defining the augmented state variable $\xi(\cdot)'=[x'(\cdot)\quad u'(\cdot)\quad x_{\mathcal{C}_k}(\cdot)']$, the augmented hybrid system is written in the form of[1]

$$\mathcal{G}_{\mathcal{C}_k}=\begin{cases}\dot{\xi}(t) &= F(t)x(t)+R_c(t)w_c(t)\\ \xi(t_k) &= H(t_k^-)\xi(t_k^-)+J_d(t_k^-)w_d[k-1]\\ z(t) &= G(t)\xi(t)+M(t)w_c(t)\end{cases} \tag{4}$$

[1]Hereafter t_k^- stands for t_{k-1}.

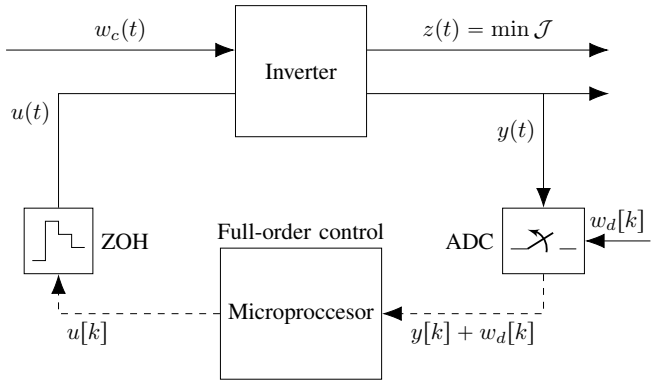

Fig. 1: General control schema based on hybrid framework.

with matrices

$$
\begin{aligned}
F(t) &= \begin{bmatrix} A(\theta(t)) & B(\theta(t)) & 0 \\ 0 & 0 & 0 \\ 0 & 0 & 0 \end{bmatrix}, \; R_c(t) = \begin{bmatrix} J(\theta(t)) \\ 0 \\ 0 \end{bmatrix}, \\
H(t_k^-) &= \begin{bmatrix} I & 0 & 0 \\ D_{\mathcal{C}_k}(\theta(t_k^-))C_y(\theta(t_k^-)) & 0 & C_{\mathcal{C}_k}(\theta(t_k^-)) \\ B_{\mathcal{C}_k}(\theta(t_k^-))C_y(\theta(t_k^-)) & 0 & A_{\mathcal{C}_k}(\theta(t_k^-)) \end{bmatrix}, \\
J_d(t_k^-) &= \begin{bmatrix} 0 \\ D_{\mathcal{C}_k}(\theta(t_k^-))E_y(\theta(t_k^-)) \\ B_{\mathcal{C}_k}(\theta(t_k^-))E_y(\theta(t_k^-)) \end{bmatrix}, \\
G(t) &= \begin{bmatrix} C_z(\theta(t)) & D_z(\theta(t)) & 0 \end{bmatrix}, \; M(t) = \begin{bmatrix} E_z(\theta(t)) \end{bmatrix}.
\end{aligned}
$$

Note that when the classic discretization methods are used, it does not reach the full mapping of the system properties. This is a key concept for obtaining realistic and representative cost functions for closed-loop systems. Generally, this cost function is based on the domain $\mathcal{L}_2$ for continuous-time cases, which refers to bounded integrable quadratic signals, while for discrete-time cases (ℓ_2) it is based on bounded summable quadratic signals. Optimizing performance in a discrete-time system and applying it to a continuous-time environment can lead to different cost values or even unstable results because the energy of the discrete signals is lower measurable due to their set strictly belonging to the $\mathcal{L}_2$ continuous-time space. Recent approaches in control and filter design for hybrid systems involve solving optimization problems based on DLMI. As far as the authors are aware, there are no synthesizing methods for DOF controllers that incorporate $\mathcal{D}$-stability constraints in this framework; therefore, this paper proposes synthesizing a guaranteed $\mathcal{D}$-stability controller in the continuous-time domain following the procedure proposed in [27][2], then the designed controller is rewritten as a discrete-time controller, following the discretization process defined in [28]. Finally, we verify the stability of the hybrid system (composed of the continuous-time model plus the discretized version of the controller) following the results from [25]. All design methods are written in the form of LMIs and DLMIs that can be solved by existing computational packages for semidefinite programming. For that purpose, consider the continuous-time DOF controller defined as

$$
\mathcal{C}_t : \begin{cases} \dot{x}_{\mathcal{C}_t}(t) = & A_{\mathcal{C}_t}(\theta(t))x_{\mathcal{C}_t}(t) + B_{\mathcal{C}_t}(\theta(t))y(t), \\ u(t) = & C_{\mathcal{C}_t}(\theta(t))x_{\mathcal{C}_t}(t) + D_{\mathcal{C}_t}(\theta(t))y(t), \end{cases} \tag{5}
$$

where $x_{\mathcal{C}_k}(t) \in \mathbb{R}^{n_c}$ is the internal state vector of the dynamic controller, which is obtained following the procedure defined in [27, Theorem 1] (hereafter called FLMOP24) to achieve performance purposes. Once the DOF controller is obtained in the form of (5), it is approximated using the procedure described in [28]. This process is based on the Taylor series expansion and the discretized system in the form of (3) has system matrices defined as

$$
\begin{aligned}
A_{\mathcal{C}_k}(\theta(t_{k-1})) &= \sum_{j=0}^{\Psi} \frac{A_{\mathcal{C}_t}(\theta(t))^j}{j!} h^j, \\
B_{\mathcal{C}_k}(\theta(t_{k-1})) &= \sum_{j=1}^{\Psi} \frac{A_{\mathcal{C}_t}(\theta(t))^{j-1}}{j!} h^j B_{\mathcal{C}_t}(\theta(t)) \\
C_{\mathcal{C}_k}(\theta(t_{k-1})) &= C_{\mathcal{C}_t}(\theta(t)), \quad D_{\mathcal{C}_k}(\theta(t_{k-1})) = D_{\mathcal{C}_t}(\theta(t)).
\end{aligned}
$$

where Ψ is the maximum degree of Taylor series expansion and h is the sampling period.

s-plane constraints for power electronics

The inverter system must not only satisfy stability or cost optimization criteria but must also hold properties in the transient performance to achieve the application requirements of such systems. In time-invariant systems, the simplest way is to generate additional constraints based on the confinement location of the eigenvalues in a limited region of the complex plane (which is known as $\mathcal{D}$-stability, more details in [27]). Fig. 2 represents a convex region formed by additional design constraints. A power electronic system (if stable) under these

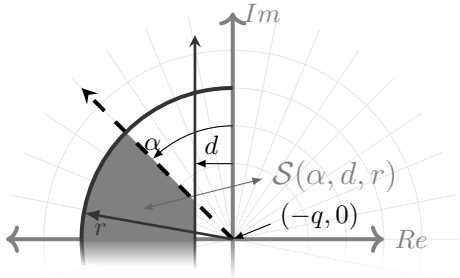

Fig. 2: Region desired $\mathcal{S}(\alpha, r, d)$ on complex plane centered in $(-q, 0)$.

constraints must primarily comply with a minimum decay rate (d) to maintain a fast time response, limited damping (bounded by α) to avoid overshoot in the state variables, and hold the dynamics below the threshold of the switching frequency (bounded by r) so that it does not contribute to the transient performance of the dynamic system. Following the classical control techniques, the selection of the exact parameters depends on the designer. A good strategy is to avoid parameters near the boundary of the desired region, since they can cause the real system to operate outside the desired performance limits.

[2]Note that in [27] a similar system was studied, where transient behavior was required, and the authors addressed the problem using an $\mathcal{H}_\infty$ performance with $\mathcal{D}$-stability constraint to supply the transient state requirement, and they obtained an acceptable behavior about the power electronic systems; for this reason, we adopted the same approach in this paper.

Sampled-data system stability verification

To verify the stability of hybrid systems in the form of (4), a well-accepted approach is the one proposed in [25], which is stated in the following lemma.

Lemma 1 (Stabilization lemma in [25]): Given $h > 0$, the hybrid system (4) is asymptotically stable if, and only if, there exists a differentiable matrix function $Q : [0, h] \to \mathbb{R}^{n+e+n_c}$ and a scalar $\epsilon > 0$ such that:

$$\begin{array}{rl} F(t)^T Q(t) + Q(t)F(t) + \dot{Q}(t) & \preceq 0 \\ H(0)^T Q(0) H(0) - Q(h) + \epsilon I & \preceq 0 \\ Q(0) & \succ 0 \end{array} \tag{6}$$

holds for all $t \in [0, h]$.
As mentioned above, the solution of the conditions from (6) can be easily reached by the usage of DLMI [26].

III. Modeling and Assumptions of an Inverter

A grid-supporting system is a microinverter used when the local microgrid is electrically weak and needs to be constantly compensated to maintain a nominal voltage amplitude and operating frequency when the system presents anomalous operation scenarios. An electrically weak grid [29], [30] is characterized by low resilience to changes in operation, that is, when the grid presents anomalous operation, its properties vary, which is an unwanted behavior. An example of this is when a load is connected to a weak grid, where due to the changes in the load, more current intensity is demanded, therefore, the voltage amplitude tends to decrease to hold the same power, and this decompensation affects the frequency of operations, which often is associated with the reactive power. In this sense, a grid-supporting system addresses a time-variant device that delivers active and reactive power to compensate for these variations while anomalous scenarios are presented.

This work addresses a grid-supporting configuration composed of an inverter and its electrical filter, which is connected to an unknown load and the local electrical grid through a connecting impedance, as seen in Fig. 3. The microgrid is emulated by a Hardware-In-the-Loop (HIL) device, and the controller is implemented on a Digital Signal Processor (DSP). It is important to mention that more complex scenarios with multiple inverters and different control issues in grid support were investigated through simulation, and the conclusions were similar to those of the simplified scenario that will be discussed in the next sections of the paper. Additionally, the authors intend to address the saturation problem in future research, since the design of controllers for hybrid systems using LMI and DLMI-based techniques is still a developing area.

A. Inverter model in state-space

The inverter state-space model can be derived by analyzing the differential equations of the RLC filter. In this model, the current and voltage in the filter are represented as vectors $i_{abc} \in \mathbb{R}^{3\times 1}$ and $v_{abc} \in \mathbb{R}^{3\times 1}$ respectively, in an abc-framework. These variables are used in the well-known Kirchhoff laws equations, which are as follows:

$$\begin{array}{ll} C_f \frac{\mathrm{d}v_{abc}(t)}{\mathrm{d}t} & = i_g(t) - i_{abc}(t), \\ L_f \frac{\mathrm{d}i_{abc}(t)}{\mathrm{d}t} & = R_f i_{abc}(t) + v_{abc}(t) - E_{abc}(t), \end{array} \tag{7}$$

where R_f, L_f, and C_f denote, respectively, the filter resistance, inductance, and capacitance. $E_{abc}(t)$ stands for the inverter output voltage. It is important to note that due to the three-phase nature of these quantities, $i_{abc}(t)$, $v_{abc}(t)$, and $E_{abc}(t)$ are all modeled as vectors.

After applying the Park and Clark transformation [31], a static framework is obtained and represented by the following differential equations

$$\begin{array}{l} \dot{v}_d(t) = \omega_0(t) v_q(t) + \frac{1}{C_f} i_d(t) - \frac{1}{C_f} I_{od}(t), \\ \dot{v}_q(t) = -\omega_0(t) v_d(t) + \frac{1}{C_f} i_q(t) - \frac{1}{C_f} I_{oq}(t), \\ \dot{i}_d(t) = \frac{R_f}{L_f} i_d(t) + \omega_0(t) i_q(t) + \frac{1}{L_f} m_d(t) - \frac{1}{L_f} v_d(t), \\ \dot{i}_q(t) = \frac{R_f}{L_f} i_q(t) - \omega_0(t) i_d(t) + \frac{1}{L_f} m_q(t) - \frac{1}{L_f} v_q(t), \end{array} \tag{8}$$

where the voltage and current are vectors of dimension 2×1 with components d and q, such that the variables $v_d(t)$, $v_q(t)$, $i_d(t)$, and $i_q(t)$ are the dq-coordinate of the filter voltage and current, respectively. The nominal operating frequency of the microgrid is represented by $\omega_0(t)$, which is time-varying in electrically weak systems, $m_d(t)$ and $m_q(t)$ are the modulation indices (switching signal function), $I_{oq}(t)$ and $I_{od}(t)$ represent the dq-coordinates of the current consumed by the load.

Consider $\tilde{x}(t) = \begin{bmatrix} v_d(t) & v_q(t) & i_d(t) & i_q(t) \end{bmatrix}'$ as the state vector, $\tilde{u}(t) = \begin{bmatrix} m_d(t) & m_q(t) \end{bmatrix}'$ as the input vector, $\tilde{w}(t) = \begin{bmatrix} I_{od}(t) & I_{oq}(t) \end{bmatrix}'$ as the disturbance input vector and $\tilde{z}(t) = \begin{bmatrix} v_d(t) & v_q(t) \end{bmatrix}'$ as the output. A state-space representation of the microgrid system illustrated by Fig. 3 is given by

$$\begin{array}{l} \dot{\tilde{x}}(t) = A(t)\tilde{x}(t) + B\tilde{u}(t) + J\tilde{w}(t), \\ \tilde{z}(t) = C_z \tilde{x}(t), \end{array} \tag{9}$$

where the matrices are

$$A(t) = \begin{bmatrix} 0 & \omega_0(t) & \frac{1}{C_f} & 0 \\ -\omega_0(t) & 0 & 0 & \frac{1}{C_f} \\ -\frac{1}{L_f} & 0 & \frac{R_f}{L_f} & \omega_0(t) \\ 0 & -\frac{1}{L_f} & -\omega_0(t) & \frac{R_f}{L_f} \end{bmatrix}, \quad B = \begin{bmatrix} 0 & 0 \\ 0 & 0 \\ \frac{1}{L_f} & 0 \\ 0 & \frac{1}{L_f} \end{bmatrix}$$

$$C_z = \begin{bmatrix} 1 & 0 & 0 & 0 \\ 0 & 1 & 0 & 0 \end{bmatrix}, \quad J = \begin{bmatrix} -\frac{1}{C_f} & 0 \\ 0 & -\frac{1}{C_f} \end{bmatrix}.$$

Note that inside the matrix $A(t)$ appears implicitly the nominal frequency $\omega_0(t)$, which is a time-varying parameter, turning it into an LPV system with affine dependency in $\omega_0(t)$. It is important to stress that the variation of $\omega_0(t)$ is dependent on the electrical condition at each instant, as was aforementioned in Section III, therefore, it is difficult to manipulate arbitrarily. Thus, the operating frequency is considered an implicit parameter, and we will only restrict ourselves to measuring it, without trying to manipulate it. Therefore, the main objective is to focus on the voltage amplitude, because it appears directly as a state signal.

IV. Control Design Methodology Description

Fig. 4 shows a general scheme of the controlled system. The upper box contains the offline algorithm that delivers as output the discrete-time matrices of the controller structure defined in (3) by $[A_{\mathcal{C}_k}, B_{\mathcal{C}_k}, C_{\mathcal{C}_k}, D_{\mathcal{C}_k}](\theta(t))$, with $\theta(t) \in \Theta$. This box has the LPV model and the $\mathcal{D}-$stable control design variables as input. For the variation of $\omega_0(t)$, by empirical knowledge, a

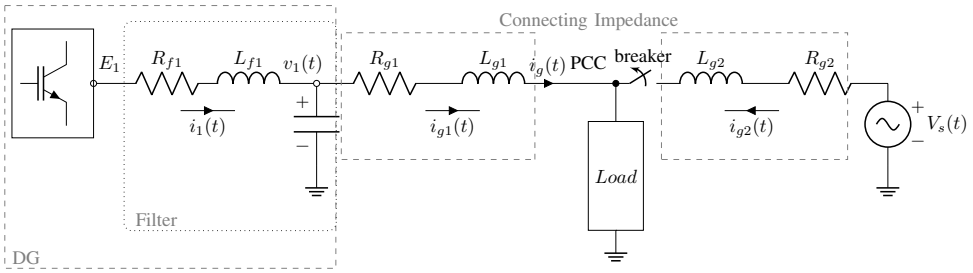

Fig. 3: Microgrid system composed of one inverter operating as a Distributed Generation (DG) unit feeding to a Point of Common Coupling (PCC) where it converges with one unknown load and the local electrical grid.

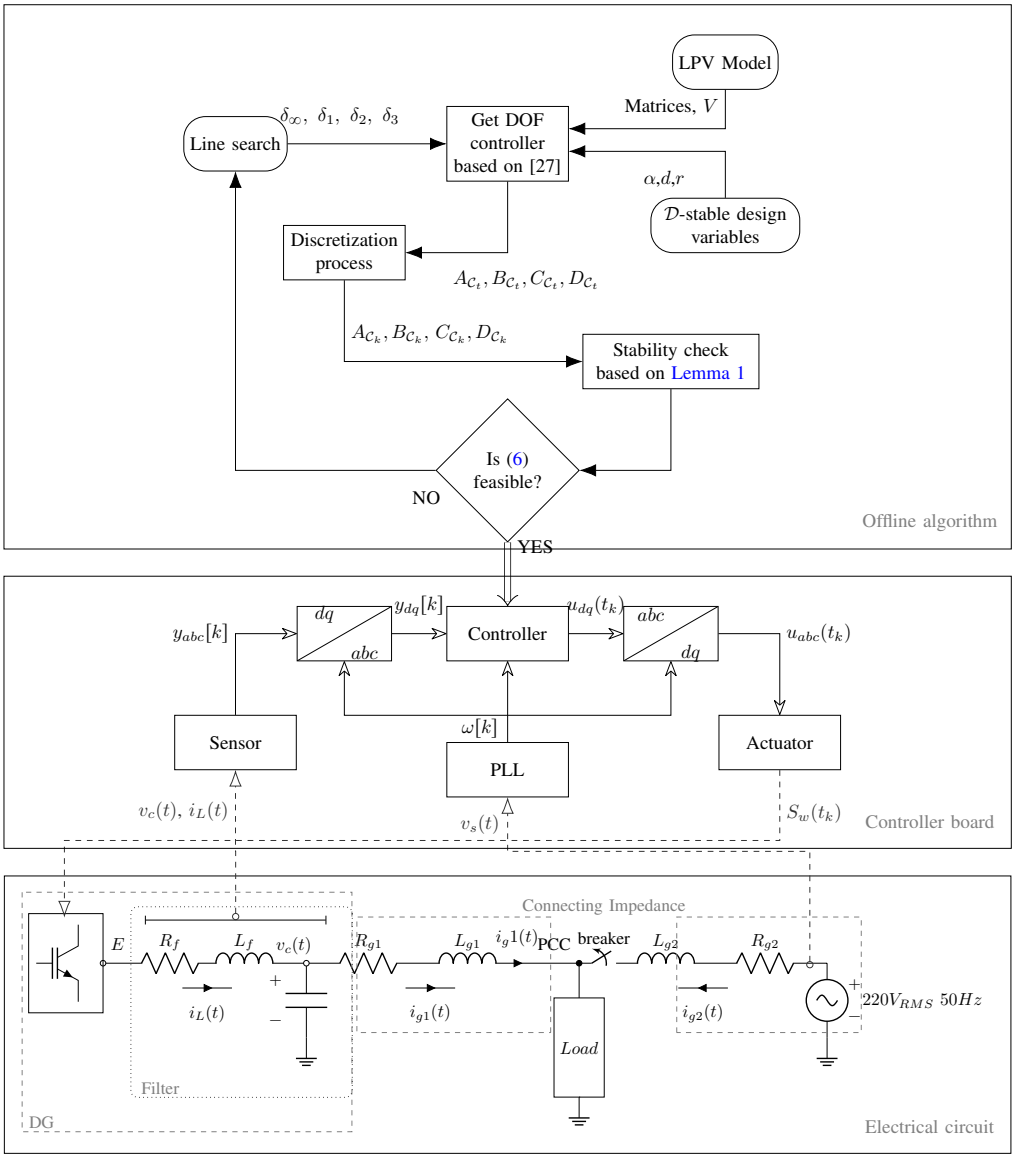

Fig. 4: Controlled system description. The upper box encloses the offline algorithm, which proves *a priori* the control gains that work *a posteriori* in the controller inside the middlebox. The state vector signal is provided by the plant, represented in the lower box.

variation of 5% with respect to the nominal value ($\omega^* = 100\pi$) is considered. The $\mathcal{D}-$stable design variables are defined based on the application and the desired transient performance. This step delivers the LPV model and the numerical values for $[\alpha, d, r]$. The next step is to solve the design method proposed in [27] to obtain the DOF continuous-time controller, which is based on a combination of relaxed LMI with a scalar search formulation in order to encompass both $\mathcal{D}$-stability and $\mathcal{H}_\infty$

criteria simultaneously. The algorithm starts a loop, iterating through all combinations of $[\delta \bigotimes \delta_1 \bigotimes \delta_2 \bigotimes \delta_3]$ with values given by Table I. Inside the loop, FLMOP24 is solved repeatedly by identifying which set of δ leads to a feasible solution and, most importantly, choosing the set that minimizes the $\mathcal{H}_\infty$ guaranteed cost given by $\sqrt{\gamma}$. The controller in continuous-time obtained from a feasible solution of FLMOP24[3] is discretized using a Taylor series expansion of one-order[4], and then employed to check Lemma 1. If it is not satisfied, the loop continues until this lemma results in a feasible solution. Once the loop has finished, the DSP performs the chosen control matrices, concluding the offline process. These discrete-time

TABLE I: Design constraint for the LMIs in [27].

	Value	Unit
f_{sw}	40	kHz
d	5 $(2\omega_0\pi)$	s^{-1}
r	$2f_{sw}\pi/10$	s^{-1}
α	$\pi/4$	rad
$\omega(t)$	$[95\pi \quad 105\pi]$	rad
δ	$[1,\cdots,9] \otimes \{10^0,\cdots,10^6\}$	
δ_1	$[1,\cdots,9] \otimes \{10^0,\cdots,10^6\}$	
δ_2	$[1,\cdots,9] \otimes \{10^0,\cdots,10^6\}$	
δ_3	$[1,\cdots,9] \otimes \{10^0,\cdots,10^6\}$	

control matrices are implemented in a DSP to work in real-time. To generate the control signal, it is necessary to handle the measurement signal and convert it from the abc-frame into the dq-frame. The control signal is then calculated, taking into account the time-varying parameter, which in this case coincides with the $\omega[k]$ signal obtained from an Enhanced Phase-Locked Loop (E-PLL) algorithm [32], [33] which provides a time response fast enough for control purposes. The use of this algorithm in this paper is also motivated by its wide employment in power electronics applications, as can be seen in [34]–[36]. Once the control signal is generated, it is transformed back into the abc-frame. Finally, the control signal is applied to the switching semiconductor device present in the plant, while the measurement is being sensed. This process is illustrated in the lower box of Fig. 4.

V. Experimental Results

A. Setup Description

Fig. 5 shows a general scheme of the test setup with the main device used. An OPAL-RT op4510 run to 10 µs is used as the HIL device, while a dSpace MicroLabBox runs the controller on 50 µs, which corresponds to the sampling time h. This sampling time was chosen because it is the minimum sampling time admitted by the DSP compiler applying the proposed control. It is important to note that this limitation is one of the motivations of this work because implementing a controller operating at a minor sampling time requires more specialized (and more expensive) hardware. On the other hand, the increase of one order of magnitude in the sampling time implies more significant distortion. The HIL device emulates

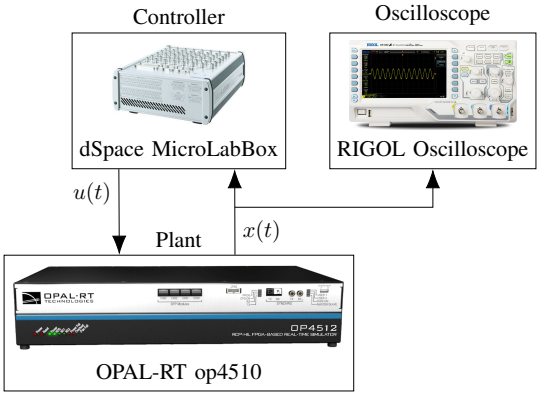

Fig. 5: Implementation schema for testing.

the system presented in Fig. 3 where the grid has a nominal voltage set in 220 V_{RMS}, the resistance, inductance and capacitance of the inverter are $R_f = 0.1\,\Omega$, $L_f = 1.35\,\text{mH}$ and $C_f = 50\,\mu\text{F}$ respectively; and constant grid frequency set in 50 Hz, such as Fig. 4. The experiment consists of the following stages:

i) The system starts feeding to a 10 kW resistive load.
ii) In the second stage, another 10 kW resistive load is connected (20 kW in total is connected).
iii) The next stage is to connect a rectified load of 10 kW (30 kW in total).
iv) Returns to the original stage (only the resistive load of 10 kW is connected).
v) In the next stage, the grid voltage decreases to 80% of the nominal voltage.
vi) The last stage is repeating the stages **ii)-iv)** for after returns to the original stages.

The above sequence presents several changes in the nominal operation that will test the performance of the proposed control strategy in anomalous scenarios, which can be too abrupt for classical control strategies, so a state-of-the-art control strategy should be used as a comparison in order to be able to point out the effectiveness of the proposal. MPC-based control strategies have performed acceptably in similar studies, therefore, we adapt the control strategy presented in [37] as a comparison.

B. Temporal results

Fig. 6 is composed of oscilloscope views that show the temporal response of the controller tested when facing the sequence of events. A view of the $dq-$frame signals during the entire sequence is presented to better see the behavior in each stage, while an $abc-$frame view of two cycles allows one to observe the signal waveform in detail. The signals plotted represent the phase-ground voltage and the current on the filter. The $dq-$frame states are reported given 10 s (10×1 s/div), where are presented the temporal response obtained by the proposed control in Fig. 6a, and the temporal response obtained by the MPC-based control strategy in Fig. 6b, while the $abc-$frame states are reported in a 50 ms (10×5 ms/div) view,

[3]Due to space limitations, all the numerical values of the system matrices and the resulting dynamic controller can be accessed at github.com/RFuentesAlbornoz/A-New-Convex-Approach-for-Grid-Supporting-Inverter-Control-Based-On-DLMIs.git .

[4]The Taylor series leads to a feasible and acceptable solution with one-order expansion (without showing significant improvement for higher-order expansions); however, in some specific cases, it may be worthwhile to enhance using a higher order.

where Fig. 6c and Fig. 6d represents the proposed control and MPC-based control, respectively.

From Fig. 6a we can notice that the voltage is maintained at the desired set point, presenting slight distortions when changes in the load or the grid voltage occur, where its last changes provide the most significant distortions. The current increases proportionally with increasing load, even when the grid voltage is not at its nominal value. The higher increase in current is shown by the decrease in the amplitude of the grid voltage. It occurs because the DG increases the current to compensate for the voltage drop of the grid, injecting power directly into the grid, in addition to the power supplied to the load.

Note that in Fig. 6b one can observe a similar temporal response on voltage signals between the proposed control and the MPC-based control, but in the current signals, the MPC-based control presented a higher noisy behavior, therefore, for precision analysis, it is necessary to conduct a harmonic study of these signals. In this sense, Fig. 7 presented a comparison of the harmonic distortion for both controllers, where Fig. 7a reports the voltage analysis, while Fig. 7b reports the harmonic distortion analysis of currents. The harmonic distortion analysis figures are plotted using data obtained directly from the oscilloscope to clarify the signal. A fundamental frequency of $50\,\mathrm{Hz}$ was considered. Fig. 7b shows a higher Total Harmonic Distortion (THD) in the current signal of the MPC-based control versus the proposed control strategy, while Fig. 7a indicates a similar behavior in the phase-ground voltage signal for both control strategies. This can be explained since MPC-based control works by minimizing a cost function, which generates a trade-off between the signals that compose the cost function. In the study, the authors adjusted the weight associated with the voltage signal as effectively as possible to achieve the lowest possible THD in voltage. This adjustment led to results comparable to those obtained with the proposed control method. However, after fitting the weight for the voltage, the authors found that they could not further reduce the THD of the currents, which present a higher THD than the proposed control. A possible explanation for this is that the proposed control incorporates more information to generate the control action. Furthermore, the proposed controller is a gain-scheduled method that better adapts to the grid frequency and parametric variations.

Fig. 8 shows the grid currents and the filter voltage in abc-frame. The correlation between the amplitude of abc and dq-frame can be validated, but the most important thing, in the zooming pictures, can be seen the alternate behavior of the phases, such that the auxiliary picture in Fig. 8a shows the currents in the main stage operation stage, remembering that they are: nominal load connected to the grid, an RL load connected to the grid, a rectified load connected, both loads disconnected, drop in the grid voltage, and again the sequential of loads connection. The zoomed picture in Fig. 8c shows that the filter maintained its voltage amplitude, even though the amplitude of the grid voltage decreased. In Fig. 8b, it is interesting to note that the convergence time of the currents is approximately 30-40ms.

VI. Conclusion

This paper presents a procedure to design an offline controller that ensures $\mathcal{D}$-stability to a sampled-data system besides validating it through experimental apparatus. The proposed algorithm considers the digital redesign of an offline DOF controller that guarantees the $\mathcal{D}$-stability of the continuous-time system; then, the discretized version of the controller is obtained; finally, an additional test to guarantee stability (provided by an approach based on DLMI) of the hybrid system (composed of the continuous-time representation of the real plant controlled by the digital version of the controller) is conducted. The experimental validation was carried out in an environment that emulated a supporting-grid inverter system, and the controller was implemented on a DSP device. The controlled grid-connected converter allows for good operation under anomalies in the voltage grid amplitude, compensating the necessary active power through the filter output current, and holding the voltage reference in distinct scenarios. The HIL results show clear signals that the controller has achieved a regular state in all load cases studied despite the anomalies presented, even regulating a voltage drop of 20%. The proposed control presents better performance than a state-of-the-art strategy concerning the THD of current, with an increase of 17.5% while holding the voltage performance. Even though the control design considers only the voltage tracking as the main design objective, i.e., when the grid-supporting problem is addressed, the proposed method based on digital re-design employs a sampled-data approach and offers an alternative to the actual solution in the literature.

Acknowledgment

This work was supported by the Chilean National Agency for Research and Development (ANID); scholarship *ANID-Doctorado* Grant N° 21232329 and N° 21231115. The ANID-Fondecyt 1241305, 1220903 and 1250838. The project Stic-Amsud AMSUD220013. The São Paulo Research Foundation (FAPESP) under grant#2024/18183-9. The Thematic Network RIBIERSE-CYTED (723RT0150). The support of the Energy Conversion Technology Center of the University of Talca.

References

[1] V. Smil, "Distributed generation and megacities: Are renewables the answer?," *IEEE Power and Energy Magazine*, vol. 17, no. 2, pp. 37–41, 2019.

[2] I. Patrao, E. Figueres, F. González-Espín, and G. Garcerá, "Transformerless topologies for grid-connected single-phase photovoltaic inverters," *Renewable and Sustainable Energy Reviews*, vol. 15, no. 7, pp. 3423–3431, 2011.

[3] B. Bahrani, "Power-synchronized grid-following inverter without a phase-locked loop," *IEEE Access*, vol. 9, pp. 112163–112176, 2021.

[4] H. Zhang, W. Xiang, W. Lin, and J. Wen, "Grid forming converters in renewable energy sources dominated power grid: Control strategy, stability, application, and challenges," *Journal of Modern Power Systems and Clean Energy*, vol. 9, no. 6, pp. 1239–1256, 2021.

[5] E. Serban, M. Ordonez, and C. Pondiche, "Voltage and frequency grid support strategies beyond standards," *IEEE Transactions on Power Electronics*, vol. 32, no. 1, pp. 298–309, 2017.

[6] A. Elnady, A. A. A. Ismail, M. AlShabi, and A. Noureldin, "A comprehensive review of centralized current/power control schemes for parallel inverters and ac microgrids," *IEEE Access*, vol. 10, pp. 125061–125085, 2022.

[7] Q. Liu, T. Caldognetto, and S. Buso, "Review and comparison of grid-tied inverter controllers in microgrids," *IEEE Transactions on Power Electronics*, vol. 35, no. 7, pp. 7624–7639, 2020.

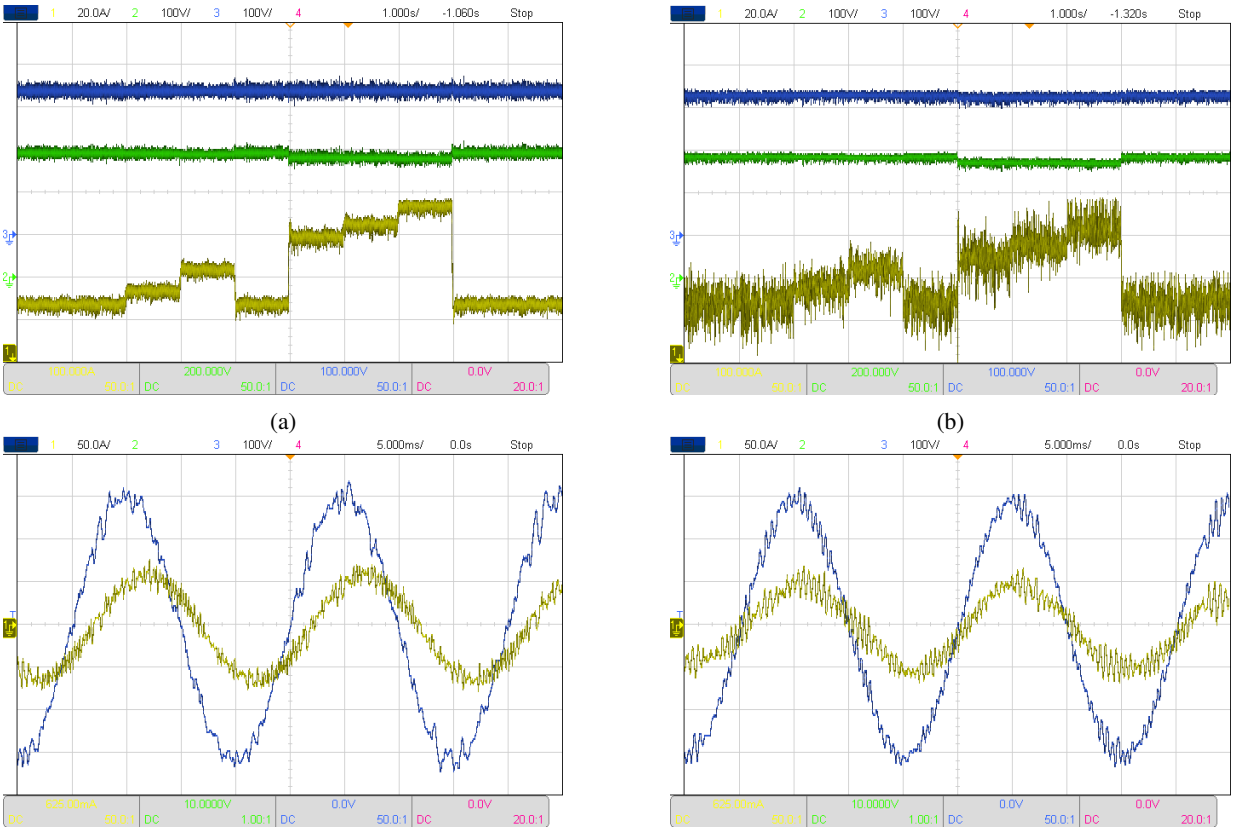

Fig. 6: Comparison between the proposed control and an MPC-based strategy. For (a) and (b) the (—) filter voltage $v_d(t)$, (—) grid voltage $v_d(t)$, and (—) filter current $i_d(t)$, and the scaling is CH1:20 A/div, CH2:100 V/div, CH3:100 V/div. For (c) and (d) the (—) represent the $a-$phase filter voltage, (—) $a-$phase filter current, and the scaling is CH1:50 A/div, CH3:100 V/div.

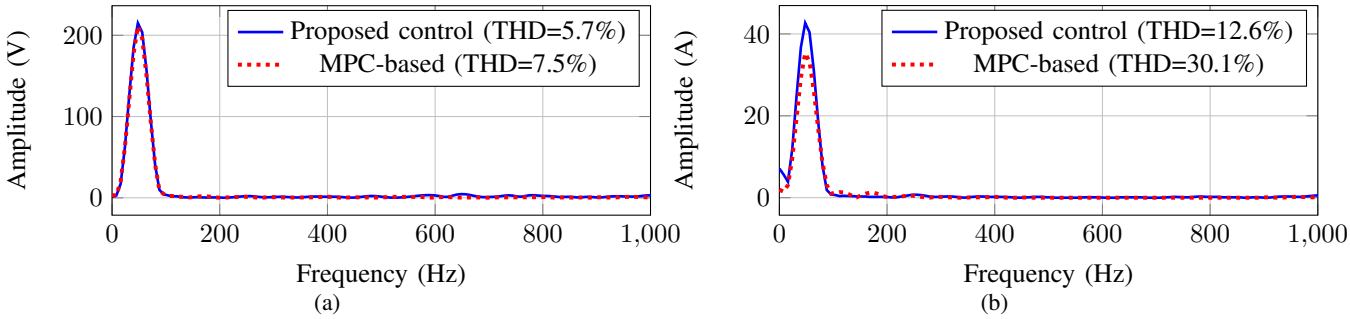

Fig. 7: THD for (a) phase-ground voltage and (b) current filter at 50 Hz as the fundamental frequency. Blue solid (—) line indicates the FFT obtained using the proposed control, and the red dotted (···) line indicates the FFT obtained employed the MPC-based control.

[8] X. Wang, P. C. Loh, and F. Blaabjerg, "Stability analysis and controller synthesis for single-loop voltage-controlled vsis," *IEEE Transactions on Power Electronics*, vol. 32, no. 9, pp. 7394–7404, 2017.

[9] Y. Tang, P. C. Loh, P. Wang, F. H. Choo, and F. Gao, "Exploring inherent damping characteristic of LCL-filters for three-phase grid-connected voltage source inverters," in *2010 IEEE Energy Conversion Congress and Exposition*, pp. 312–319, 2010.

[10] Z. Xin, X. Wang, P. C. Loh, and F. Blaabjerg, "Grid-current-feedback control for LCL-filtered grid converters with enhanced stability," *IEEE Transactions on Power Electronics*, vol. 32, no. 4, pp. 3216–3228, 2017.

[11] X. Guo, W. Liu, and Z. Lu, "Flexible power regulation and current-limited control of the grid-connected inverter under unbalanced grid voltage faults," *IEEE Transactions on Industrial Electronics*, vol. 64, no. 9, pp. 7425–7432, 2017.

[12] S. Vadi and R. Bayindir, "Modeling, analysis and proportional resonant and proportional integral based control strategy for single phase quasi-z source inverters," *IEEE Access*, vol. 10, pp. 87217–87226, 2022.

[13] X. Quan, "Improved dynamic response design for proportional resonant control applied to three-phase grid-forming inverter," *IEEE Transactions on Industrial Electronics*, vol. 68, no. 10, pp. 9919–9930, 2021.

[14] S. Buso, T. Caldognetto, and D. I. Brandao, "Dead-beat current controller for voltage-source converters with improved large-signal response," *IEEE Transactions on Industry Applications*, vol. 52, no. 2, pp. 1588–1596, 2016.

[15] S. Wei, Z. Zhao, K. Li, L. Yuan, and W. Wen, "Deadbeat current controller for bidirectional dual-active-bridge converter using an enhanced sps modulation method," *IEEE Transactions on Power Electronics*, vol. 36, no. 2, pp. 1274–1279, 2021.

[16] C. R. Baier, R. O. Ramirez, E. I. Marciel, J. C. Hernández, P. E. Melín, and E. E. Espinosa, "FCS-MPC without steady-state error applied to a grid-connected cascaded H-bridge multilevel inverter," *IEEE Transactions on Power Electronics*, vol. 36, no. 10, pp. 11785–11799, 2021.

[17] X. Chen, Y. Zhang, S. Wang, J. Chen, and C. Gong, "Impedance-phased dynamic control method for grid-connected inverters in a weak grid," *IEEE Transactions on Power Electronics*, vol. 32, no. 1, pp. 274–283, 2017.

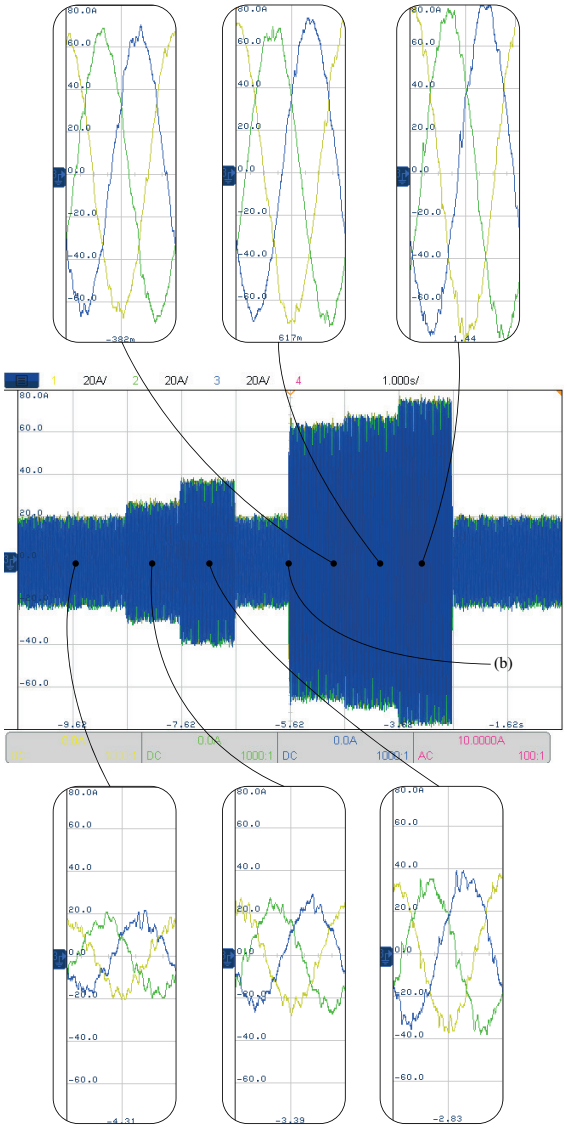

(a) Grid current in *abc*-frame with zooming of the main stages of operation.

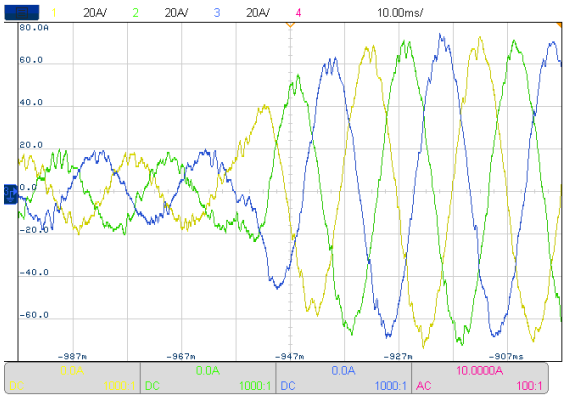

(b) Zooming in on the transition between the nominal grid voltage operation to the anomalous grid voltage operation.

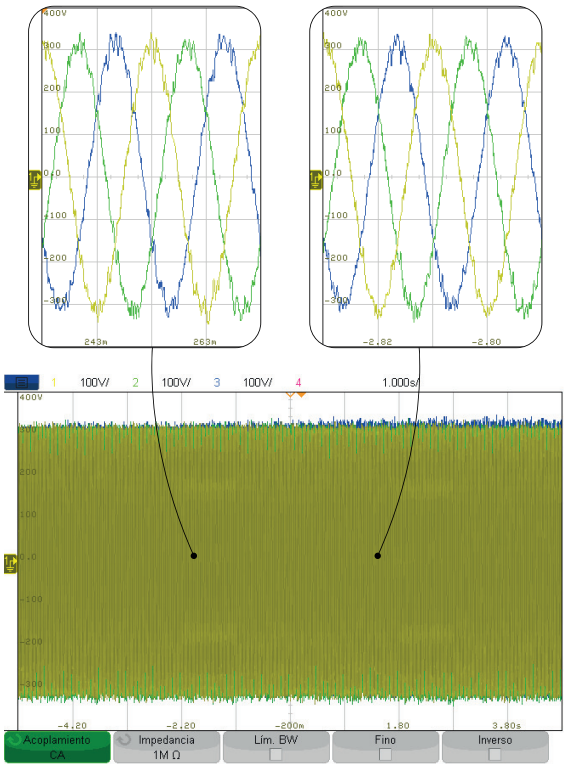

(c) Filter voltage in the whole study period with zooming in on the nominal and the anomalous grid operation.

Fig. 8: States of the inverter in *abc*-frame. The phases a, b and c are represented by (—), (—), and (—), respectively. (a) and (b) present a scaling of 20 A/div, and (c) present a scaling of 100 V/div. The time scale is of 1 s/div for mains figures, and the zooming pictures are time-scaled to 10 ms/div.

[18] J. Andino, P. Ayala, J. Llanos-Proaño, D. Naunay, W. Martinez, and D. Arcos-Aviles, "Constrained modulated model predictive control for a three-phase three-level voltage source inverter," *IEEE Access*, vol. 10, pp. 10673–10687, 2022.

[19] F. Khosrosereshki and B. Moaveni, "Model validation and robust state feedback control for nonlinear subway traffic networks," *ISA Transactions*, vol. 148, pp. 12–23, 2024.

[20] F. Thomas and M. S.J., "Output feedback based adaptive composite nonlinear flight control design for a small-scale un-crewed helicopter," *ISA Transactions*, vol. 126, pp. 190–202, 2022.

[21] A. Kazemy, Éva Gyurkovics, and T. Takács, "Dynamic output feedback h∞ design in finite-frequency domain for constrained linear systems," *ISA Transactions*, vol. 96, pp. 185–194, 2020.

[22] H. Yao and F. Gao, "Design of observer and dynamic output feedback control for fuzzy networked systems," *Mathematics*, vol. 11, no. 1, 2023.

[23] J. C. Geromel, P. Colaneri, and P. Bolzern, "Differential linear matrix inequality in optimal sampled-data control," *Automatica*, vol. 100, pp. 289–298, 2019.

[24] H. W. Pereira, G. W. Gabriel, A. M. de Oliveira, and J. C. Geromel, "Differential linear matrix inequalities in optimal and robust sampled-data filtering," *IFAC-PapersOnLine*, vol. 56, no. 2, pp. 9806–9811, 2023. 22nd IFAC World Congress.

[25] C. Briat, "Convex conditions for robust stability analysis and stabilization of linear aperiodic impulsive and sampled-data systems under dwell-time constraints," *Automatica*, vol. 49, no. 11, pp. 3449–3457, 2013.

[26] T. R. Gonçalves, G. W. Gabriel, and J. C. Geromel, "Differential linear matrix inequalities optimization," *IEEE Control Systems Letters*, vol. 3, no. 2, pp. 380–385, 2019.

[27] R. Fuentes, M. Lacerda, C. Morais, R. Oliveira, and J. Palma, "$\mathcal{H}_\infty$ gain-scheduled dynamic output feedback control with transient performance applied to electrical microgrid," *Journal of the Franklin Institute*, p. 106704, 2024.

[28] M. F. Braga, C. F. Morais, E. S. Tognetti, R. C. L. F. Oliveira, and P. L. D. Peres, "A new procedure for discretization and state feedback control of uncertain linear systems," in *52nd IEEE Conference on Decision and Control*, pp. 6397–6402, 2013.

[29] C. Li, W. Liu, J. Liang, X. Ding, and L. M. Cipcigan, "Improved grid impedance compensation for phase-locked loop to stabilize the very-weak-grid connection of VSIs," *IEEE Transactions on Power Delivery*, vol. 37, no. 5, pp. 3863–3872, 2022.
[30] Y. Li, L. Fan, and Z. Miao, "Wind in weak grids: Low-frequency oscillations, subsynchronous oscillations, and torsional interactions," *IEEE Transactions on Power Systems*, vol. 35, no. 1, pp. 109–118, 2020.
[31] T. Hao, F. Gao, and T. Xu, "Fast symmetrical component extraction from unbalanced three-phase signals using non-nominal dq -transformation," *IEEE Transactions on Power Electronics*, vol. 33, no. 11, pp. 9134–9141, 2018.
[32] M. Karimi-Ghartemani and M. Iravani, "A nonlinear adaptive filter for online signal analysis in power systems: applications," *IEEE Transactions on Power Delivery*, vol. 17, no. 2, pp. 617–622, 2002.
[33] M. Karimi-Ghartema, *Enhanced phase-locked loop structures for power and energy applications*. John Wiley & Sons, 2014.
[34] S. Kumar, R. Sreejith, and B. Singh, "Sensorless pmsm ev drive using modified enhanced PLL based sliding mode observer," in *2021 International Conference on Sustainable Energy and Future Electric Transportation (SEFET)*, pp. 1–6, IEEE, 2021.
[35] R. Hariharan and M. K. Mishra, "An integrated control of enhanced-PLL and synchronverter for unbalanced grid," *IEEE Transactions on Industry Applications*, vol. 58, no. 2, pp. 2206–2216, 2021.
[36] M. Eskandari, A. V. Savkin, H. H. Alhelou, and F. Blaabjerg, "Explicit impedance modeling and shaping of grid-connected converters via an enhanced PLL for stabilizing the weak grid connection," *IEEE Access*, vol. 10, pp. 128874–128889, 2022.
[37] H. A. Young, V. A. Marin, C. Pesce, and J. Rodriguez, "Simple finite-control-set model predictive control of grid-forming inverters with LCL filters," *IEEE Access*, vol. 8, pp. 81246–81256, 2020.

Roberto M. Fuentes received the B.S. and M.S. degrees in Engineering Science at the University of Talca, Curicó, Chile, in 2021 and 2023, respectively. He is currently working toward the Ph.D. degree in Engineering Systems at the University of Talca, Curicó, Chile. His research interests mainly include robust stability analysis and control of uncertain sampled-data linear systems, and markov jump linear systems.

Esteban I. Marciel received the B.Sc. and Engineer degrees in Mechatronics in 2018 and 2020, respectively, from the University of Talca, Talca, Chile. He received the M.Sc. degree in Engineering Sciences with a specialization in Energy Conversion in 2023 from the University of Talca, where he is currently pursuing the Ph.D. degree in Engineering Systems. His research interests include multicell power converters, grid-forming converters, emerging converter topologies, and hybrid transformers.

Carlos R. Baier (Senior Member, IEEE) received the B.S., M.Sc., and D.Sc. degrees in electrical engineering from the University of Concepción, Concepción, Chile, in 2004, 2006, and 2010, respectively. Since 2009, he has been a Professor with the Faculty of Engineering at Universidad de Talca, Curicó, Chile, where he teaches in the area of industrial electronics. His research interests include improved control techniques for multicell converters, emerging converters and strategies to inject power into the grid, and high energy efficient improvements for medium-voltage converters.

Gabriela W. Gabriel has received her B.S. degree in Electronic Engineering from Instituto Tecnológico de Aeronáutica (ITA), Brazil, in 2003, her M.Sc. degree from ITA, Brazil, in 2005; and her Doctor in Engineering degree in 2016, from UNICAMP. During her doctorate, she did a Research internship at the University of Houston, Texas, USA, and conducted post-doctoral research at UNICAMP from 2016 to 2018. From 2006 to 2013, she worked at PADTEC S.A., Brazil, as a firmware developer and as a project manager, concluding her MBA in Project Management from Fundação Getulio Vargas - FGV, Brazil, in 2007. Since 2018, she has been a professor of Control theory at ITA and integrates the Post-graduation Programs PG/EEC and PEE-Embraer. Her research interests are on topics related to Networked Control Systems (NCS), Optimal Control applied to Hybrid Systems, as well as applications on eVTOLs and aircraft identification and control.

Cecilia F. Morais received her BSc degree in Electrical Engineering from the Federal University of Goiás, GO, Brazil, in 2009, and her MSc and Phd degrees in Electrical Engineering from the University of Campinas (UNICAMP), SP, Brazil, in 2011 and 2015, respectively. She held a postdoc position at the School of Electrical and Computer Engineering (FEEC), UNICAMP, from February 2015 to December 2019. She worked as a Professor and Researcher at the Polytechnic School of the Pontifical Catholic University of Campinas (PUC-Campinas) and at the Graduate Program in Electrical Engineering (Professional Master's Degree in Telecommunications Network Management) at PUC-Campinas from December 2019 to June 2024. She is currently Professor I (MS3.1) at the Department of Systems and Energy (DSE) of FEEC-UNICAMP. Her research interests include digital control design of dynamical systems, robust stability analysis, and control of: Uncertain, Linear Parameter Varying, and Markov Jump Linear Systems.

Marcio J. Lacerda is a Reader in Control Engineering and Cyber–Physical Systems at London Metropolitan University. Previously, he was with the Federal University of São João del-Rei, Brazil (2016–2023) and held postdoctoral positions at UNICAMP and the University of Minnesota. He earned his Ph.D. in Electrical Engineering from UNICAMP in 2014. He is a Senior Member of the IEEE and holds editorial roles on the Conference Editorial Board and Technology Conference Editorial Board of the IEEE Control Systems Society. Additionally, he serves as an Associate Editor for the Journal of Control Automation and Electrical Systems. His research focuses on constrained control, robust control, and cyber–physical systems.

Jonathan M. Palma Jonathan Matías Palma Olate is an Assistant Professor in the Department of Electrical Engineering at the Universidad de Talca, Chile, and head of the Laboratory of Automated Systems. His work lies at the intersection of control theory and cyber-physical systems, with interests in sampled-data and hybrid systems, LPV and Markov jump linear systems (MJLS), robust filtering, and networked control. He applies these methods to power and energy processes as well as biomedical/pharmacokinetic problems. He teaches courses in control systems and advisor undergraduate, master's, and Ph.D. students.